IAES International Journal of Robotics and Automation (IJRA)
Vol. 15, No. 2, June 2026, pp. 267∼280
ISSN: 2722-2586, DOI: 10.11591/ijra.v15i2.pp267-280

Development of a low pressure Pneu-Nets actuator using room temperature vulcanizing silicon rubber

Nur Rahmah Abdullah[1], Sylvi Febriana Rachmawati Irnadiastputri[1,2], Mohammad Ikhsan[1,2]
[1]Department of Electrical Engineering, Faculty of Engineering, Universitas Indonesia, Depok Indonesia
[2]Research Center for Biomedical Engineering, Faculty of Engineering, Universitas Indonesia, Depok, Indonesia

Article Info

Article history:

Received Jun 16, 2025
Revised Nov 21, 2025
Accepted Mar 6, 2026

Keywords:

Finite element analysis
Pneu-Nets actuator
RTV silicone rubber
Soft robotics
Wearable robotics

ABSTRACT

Soft robotics offers potential advantages in achieving safer human-robot interaction compared to conventional rigid robots, making it relevant for stroke rehabilitation applications. A major challenge in developing soft actuators lies in selecting materials that balance mechanical performance and practical fabrication. This study investigates room-temperature vulcanizing (RTV) silicone rubber as an alternative to platinum-cured silicone rubber for Pneumatic-Networks (Pneu-Nets) actuators fabrication. The actuator was developed through mold casting with 3D-printed molds and characterized by its contact force and bending angle. This actuator produced a maximum force of 0.93 N and a bending angle of 244.5° at 52 kPa. Finite element analysis (FEA) was performed to simulate its mechanical behavior and validate experimental results. The simulation errors were quantified as 8.3% for contact force and 19.3% for bending angle at 30 kPa, confirming the feasibility of using condensation-cured silicone rubber for efficient soft actuator production.

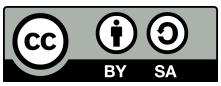

Corresponding Author:

Mohammad Ikhsan
Department of Electrical Engineering, Faculty of Engineering, Universitas Indonesia
Depok, West Java, Indonesia
Email: mohammad.ikhsan04@ui.ac.id

1. INTRODUCTION

Stroke is a neurological disorder characterized by the interruption of blood flow to the brain, leading to the abrupt death of neuronal cells and consequent damage to cerebral tissue [1]. The Global Burden of Disease (GBD) estimated that 13.7 million people experience strokes annually [1]–[4]. Hemiplegia, a common post-stroke symptom, is characterized by unilateral paralysis that impairs motor coordination and mostly affects upper extremities, with approximately 75% of cases among all stroke patients [4], [5].

Motor function restoration in post-stroke patients mostly relies on repetitive physical therapy, which is designed to improve muscle strength and increase range of motion (ROM). Motor recovery commonly occurs within three to six months after stroke onset, in line with a critical period of neuroplasticity. Dromerick *et al.* [6] reported that there is a sensitive window for effective motor rehabilitation between 60 and 90 days post-stroke. Within this phase, an intensive therapy offers the greatest improvements. In contrast, beyond six month, the therapy efficacy will reduced. However, only about 25% of stroke survivors regain their ability to perform activities of daily living (ADLs), while approximately 65% of them are unable to effectively use their paretic (affected) hand even six months after onset [7]. Thus, assistive hand rehabilitation technologies are urgently needed to support long-term hand function and independence.

Robotic rehabilitation systems have been designed to restore motor function in post-stroke patients

through consistent, measurable training sessions. These systems enhance movement control and agility, facilitating the patient's ability to perform daily tasks independently. Additionally, it also alleviates therapists' workloads by automating repetitive tasks. By applying this scheme, the treatment efficiency and patient care will be improved [8]. The integration of repetitive therapy with robotic assistive devices, such as exoskeletons, can improve training efficiency. However, movement facilitated by the exoskeleton exhibits a limited range of motion, which may restrict natural limb kinematics during rehabilitation [9]–[12].

Soft robotics refers to systems that modify conventional robotic mechanism by using low-modulus material such as elastomer, resulting in smoother and more harmonious motion compared to conventional robots. These robots also provide safer interactions, as forces are evenly distributed across their surface. Another advantage of soft robots lies in their adaptability to various operational environments, which enables them to perform a variety of motions, including bending, twisting, and telescoping [13]–[15]. These systems operate based on the integrated actuator. Soft fluidic actuators (SFAs) operate through pressurize fluid within the internal chambers. Pneumatic networks (Pneu-Nets) actuators, a notable type of SFAs, comprise interconnected chambers connected by an internal channel that facilitate precise actuation control. This system is active when pressurized air inflates the chambers through this channel [16].

The material selection plays a role in the actuator performance, as the mechanical properties of these materials significantly influence deformation [17]. Elastomers like thermoplastic polyurethane (TPU) and silicone rubber are commonly used in the fabrication of Pneu-Nets actuators due to their flexibility. Platinum-cured silicone rubber is the most commonly used material due to its durability. However, this material is sensitive to temperature changes and chemical inhibitors during curing, which may affect the mechanical performance of Pneu-Nets actuators. Condensation-cured silicone rubber offers stable thermal properties and faster curing, making it a promising alternative [18].

The structural design of the actuator also plays a critical role in optimizing movement flexibility and patient comfort during rehabilitation training [19]. Hu *et al.* [20] showed that chamber configuration significantly influences actuator performance through stress and deformation distribution. Poor chamber configurations may demand higher pressure, accelerating material fatigue under cyclic loading conditions.

The Pneu-Nets actuator performances vary widely within their geometry, material, and pressure input. Table 1 compares some previous studies, emphasizing the importance of material and configuration in mechanical performance. Actuators fabricated from platinum-cured silicones achieved bending angles between 90° and 180° with maximum force outputs ranging from 0.65 to 2.39 N. In contrast, the condensation-cured silicone actuator produced 1.2 to 1.43 N under higher input pressure.

Table 1. Comparison of reported Pneu-Nets actuator performance in literature

Material	Geometry Type	Pressure (kPa)	Max Bending Angle (°)	Max Force (N)	Ref.
Platinum-cured	Semi-circular with additional strain layer	0–50	90	0.75	[21]
Platinum-cured	Semi-circular chamber	0–80	120	0.65	[22]
Platinum-cured	Variable chamber volume	0–120	180	2.39	[23]
Condesation-cured	Plate inter-chamber	0–300	120	1.43	[24]
Condesation-cured	Flat-pinch end	0–105	70	1.2	[25]

This study examines the feasibility of using room-temperature vulcanizing (RTV) silicone rubber, a condensation-cured silicone, as an alternative material for fabricating Pneu-Nets actuators intended for soft rehabilitation robotics. The actuator's performance is assessed through experimental characterization and compared with finite element analysis (FEA) simulations. Section 2 details the actuator geometry, material properties, fabrication process, and characterization methodology. Section 3 presents the experimental results and discussion. Section 4 concludes the study and suggests directions for future research.

2. METHOD

2.1. Design of Pneu-Nets actuators

Pneu-Nets actuators consist of a multi-chambered structure arranged in series, enabling uniform bending behavior under low input pressures. Bending motion is a result of the differential stiffness between the upper

and lower layers of the actuator. One of the effective strategies for optimizing the actuator performance is by adjusting the thickness of these layers [17], [26].

This study adapts the soft gripper design proposed by Zhong *et al.* [22] by applying a semi-circular chamber configuration to generate a large bending angle under low-pressure intake. In this study, the geometry was modified to match hand rehabilitation applications.

The proposed Pneu-Nets actuator design features an optimized geometry with overall dimensions of 100 mm (length), 20 mm (width), and 20 mm (height), as illustrated in Figure 1. This dimension was selected to approximate the average phalange length of Asian adults (70-80 mm) [27], ensuring ergonomic compatibility for finger rehabilitation. The actuator consists of ten serially arranged chambers. The terminal chamber is 6 mm wide, while the other nine chambers are each 3.5 mm wide. The enlarged terminal chamber was designed to enhance the tip-force output and mimic the tips of human fingers. Each chamber adopts a semi-circular cross-section with an inner radius of 8 mm and an outer radius of 10 mm to optimize stress distribution and deformation. Hu *et al.* [20] reported that a half-round structure produces a higher bending angle compared to rectangular geometry. This configuration also lowers stress concentration and provides better resistance to local buckling, extending the actuator life under cyclic operation.

A stiffness gradient was achieved by varying layer thickness (4 mm base and 3 mm upper). This configuration was established through experimental evaluation following multiple fabrication trials. Preliminary tests revealed that the 2 mm upper-layer actuator experienced a rupture under inflation, indicating a poor stress distribution. The final 4-3 mm configuration offered a balance between flexibility and structural durability, ensuring stable deformation without material failure. Unlike the gripper design by Zhong *et al.* [22], this actuator eliminates additional structural convex edges, maintaining a uniform stress distribution across the chamber walls.

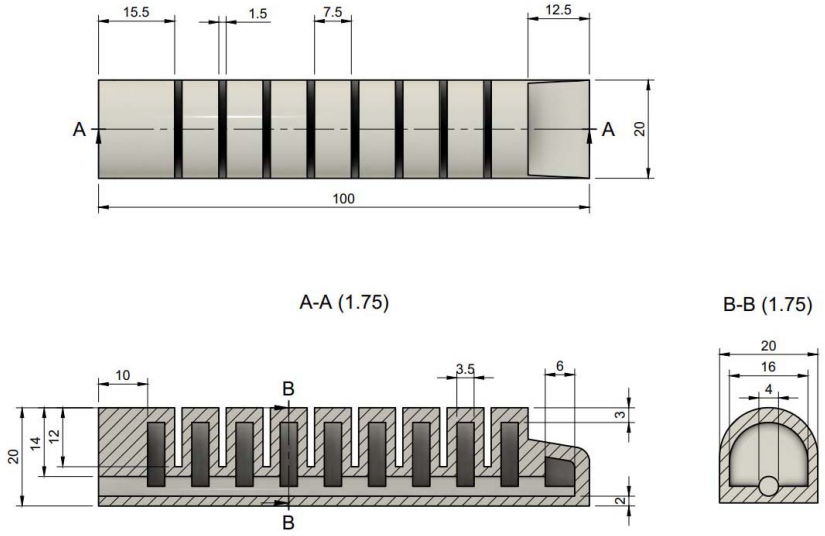

Figure 1. Dimensional schematic of the Pneu-Nets soft actuator (all dimensions in mm)

2.2. Fabrication

Mold casting is the most common method for fabricating Pneu-Nets actuators, enabling precise and complex geometries [28], [29]. In this study, molds were designed using computer-aided design (CAD) software and were then printed with polylactic acid (PLA) filament on a Bambu Lab X1 printer. The nozzle diameter of 0.4 mm produces a dimensional tolerance of ±0.2 mm.

Material selection focused on materials with strain-tolerant and fatigue-resistant characteristics to ensure shape recovery after repeated actuation cycles while maintaining structural integrity [30]. Silicone rubber, a synthetic elastomer with siloxane (Si-O) backbone structures, offers biocompatibility, thermal resistance, and chemical resistance. Platinum-cured silicone rubber is widely used due to its reliable curing process and stability. Some of them are Dragon Skin 10, Dragon Skin 30, Ecoflex 00-30, and Ecoflex 00-50, which exhibit Shore A hardness values ranging from 0 to 50 A [18].

Condensation-cured silicone rubber forms through a condensation reaction between hydroxyl-terminated

polydimethylsiloxane (HO-PDMS-OH) and a hydrolyzable silane crosslinker. This process allows curing under ambient conditions, offering a significant advantage over platinum-cured silicone rubbers, which generally require a controlled environment [31], [32]. Room-temperature vulcanizing (RTV) silicone rubber, which is a condensation-cured silicone rubber, was used in this study. The selected RTV has a Shore hardness of 48 A and an elastic modulus of 12.81 psi. Table 2 presents the mechanical properties of silicone rubbers used for soft robot applications.

Table 2. Material properties of elastomer [16]

Materials	Shore Hardness (A)	100% Modulus (psi)	Cure Time (min)
	Platinum-cured silicone rubber		
Dragon skin 30 A	30	86	960
Ecoflex 00-30	00-30	10	240
Ecoflex 00-50	00-50	12	180
	Condensation-cured silicone rubber		
Mold star 30	30	96	960
Mold max 40	40	190	1440

The fabrication process of the Pneu-Nets actuator is illustrated in Figure 2. RTV silicone rubber and a catalyst with a weight ratio of 1:0.04 were mixed and poured into the mold cavity up to 90% of its volume. When the upper mold was closed, a small amount of excess silicone overflowed from the mold edges, allowing the trapped air inside to escape simultaneously. This method was adopted to compensate for the inability to inspect internal bubbles in closed-mold casting. After one hour of curing, the actuator components were demolded, and any excess silicone was trimmed. The chamber and cover layer were bonded using the same mixture as an adhesive, maintaining uniformity in material. Minor air leakage from incomplete sealing was addressed by applying more silicone and extending the bonding process by one hour. A 3D-printed pipe was inserted into the actuator inlet to reduce air leakage. This connector was sealed using the same mixture and cured for one hour. To ensure stability and limit leakage, the port is then reinforced using seal tape and Kevlar thread.

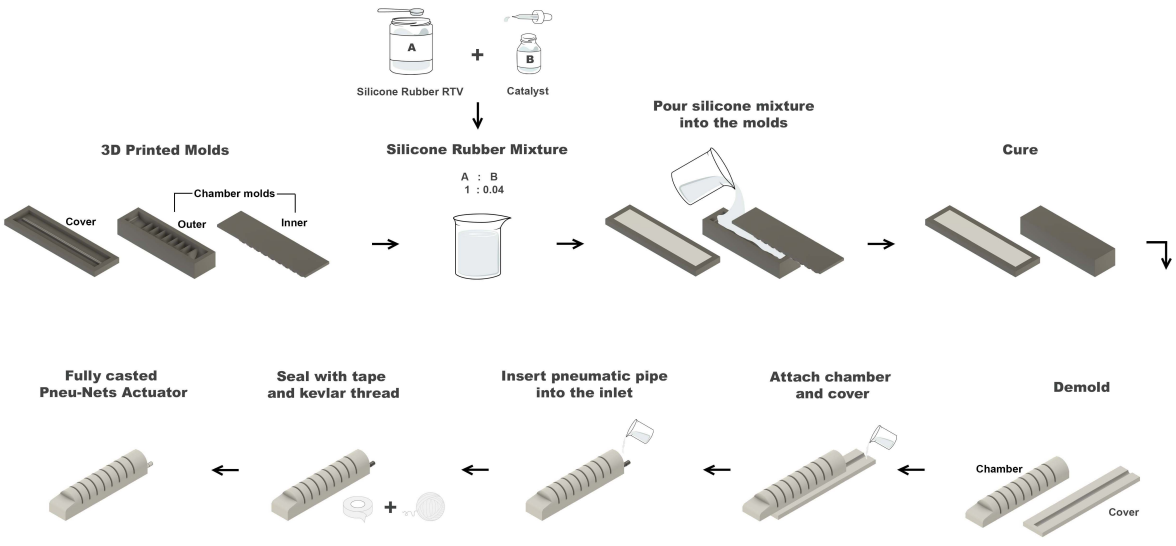

Figure 2. The fabrication process of the Pneu-Nets actuator

Closed-mold techniques demonstrated good reproducibility, with dimensional variation within 3% due to printer tolerance and minor shrinkage during curing. Challenges such as air bubble entrapment and incomplete bonding between layers were addressed by controlling the silicone rubber mixture. Despite these issues, the actuators managed to have smooth surfaces and consistent mechanical properties.

2.3. Mechanical characterization of RTV 48 silicone rubber

The mechanical response of RTV 48 A silicone rubber was characterized through uniaxial tensile testing to obtain the mechanical characteristics required for finite element analysis (FEA) simulations of the Pneu-Nets actuator. The dumbbell-shaped specimens were molded to ASTM D412 Type C geometry and tested under quasi-static, room-temperature conditions on an Instron 5900 universal testing machine. A total of three specimens were tested, and the average curve was used to represent the material's behavior. Each specimen was measured individually to ensure consistency. The force-displacement data obtained from the test were converted into stress-strain curves, as illustrated in Figure 3, from which key properties were extracted.

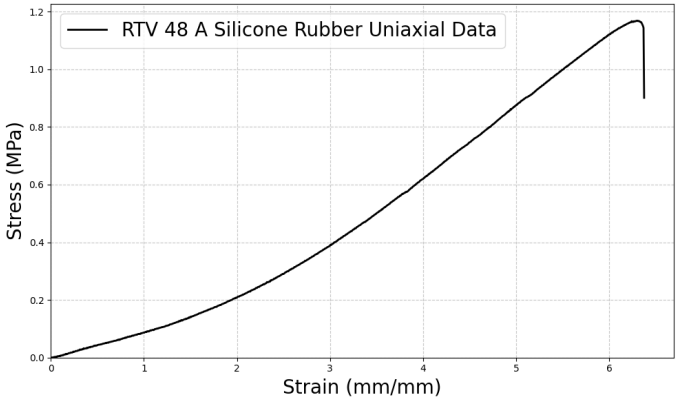

Figure 3. Stress-strain relationship of RTV 48 A silicone rubber

The mechanical properties of RTV 48 silicone rubber are summarized in Table 3. RTV 48 A exhibited a density of 1434 kg/m^3 and a 100% modulus value of 0.088 MPa (12.81 psi). Like most silicone elastomers, RTV 48 A silicone rubber exhibits nearly incompressible behavior, which was represented by an assumed Poisson's ratio of 0.5. This assumption is supported by previous studies by Li *et al.* [33] and Ilg *et al.* [34], who reported similar values for silicone rubber. In this study, a value of 0.499 was used to ensure numerical stability in finite element simulation, because the exact value of 0.5 cannot be implemented in ANSYS due to matrix singularity issues. These experimental data were subsequently fitted using a Neo-Hookean hyperelastic model to describe the non-linear elastic behavior under large deformations, which was subsequently employed during the design of the Pneu-Nets actuator.

Table 3. Mechanical Properties of RTV 48 A Silicone Rubber

Property	Value	Unit
Density	1 434	kg m^{-3}
Isotropic Elasticity Characteristics		
Young's modulus	0.088	MPa
Poisson's ratio	0.499	
Bulk modulus	2.103×10^6	Pa
Shear modulus	29579	Pa
Hyperelastic Characteristics		
Neo-Hookean initial shear modulus	1340	Pa

2.4. Finite element analysis

Finite element analysis was performed using ANSYS to predict the actuator's kinematics, output force, deformation profile, and internal stress distribution. The actuator was modeled in Autodesk Fusion 360 and imported into ANSYS. A tetrahedral mesh was adopted due of its ability to capture the non-linear behavior of the elastomer. A mesh convergence study was achieved by refining the element size from 4 mm to 3 mm, with smaller sizes excluded due to computational cost and negligible gains. The final mesh configuration consists of 24,700 nodes and 14,200 elements.

For the contact force simulation, the actuator was placed above the load cell, as illustrated in Figure 4(a). The interface between the actuator and the load cell is defined as the contact region and was modeled as frictionless. This area is presented in Figure 4(b) to 4(c). Fixed support was assigned both on the load cell and actuator base, as shown in Figure 4(d), and internal pressure was applied to the actuator chambers as illustrated in Figure 4(e).

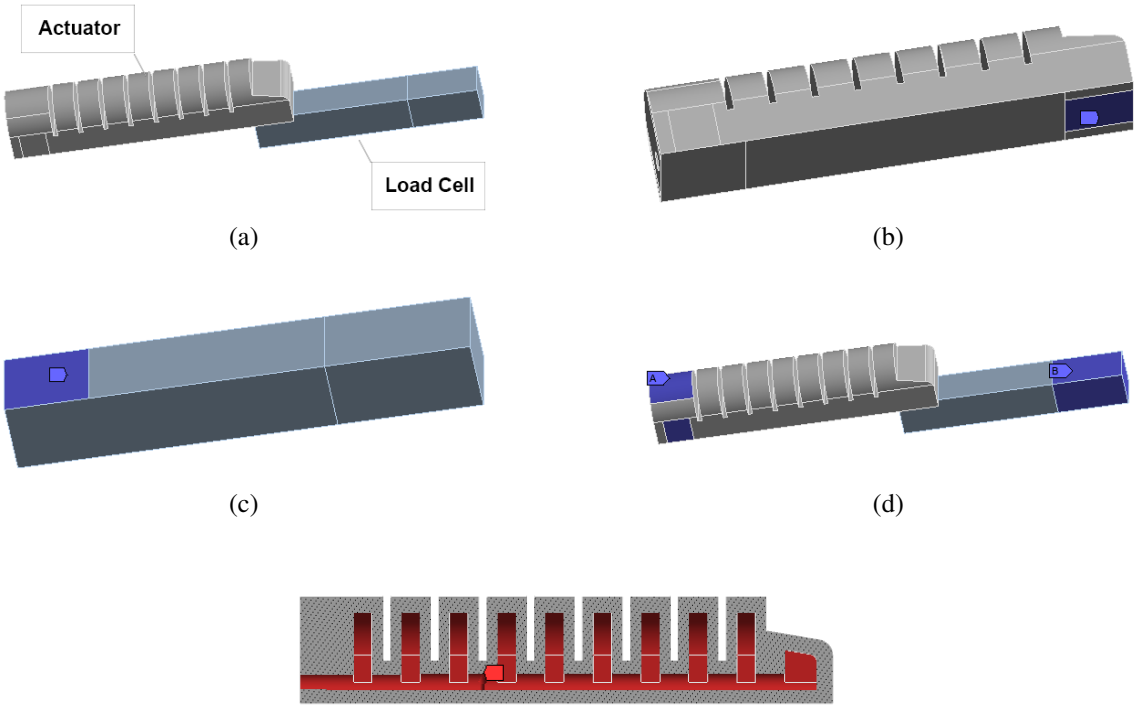

Figure 4. Simulation setup for contact force analysis: (a) contact force setup, (b) fixed support for actuator and load cell, (c) air pressure input, (d) actuator contact region, and (e) load cell contact region

2.5. Experimental and characterization of the actuator

The performance of the Pneu-Nets actuator was evaluated through experiments that were designed to replicate human finger movements. These evaluations consist of contact force and bending angle. The experimental setup for these measurements is illustrated in Figure 5. The actuator was tested using air pressure from 0 to 52 kPa, with increments of 2 kPa. The input pressure was controlled via pulse-width modulation (PWM) and monitored in real-time using a pressure sensor (WPT-83 G). The complete configuration of the experimental system is shown in Figure 5(a). In the simulation, the FEA was limited to 30 kPa due to numerical constraints. However, within this range, the system still managed to capture the initial response of the actuator.

The contact force test evaluated the Pneu-Nets actuator's ability to assist hand gripping tasks and support patient rehabilitation [19], [24], [35]. The actuator tip was positioned above a load cell. When the actuation began, the actuator bent and exerted a force on the load cell. This procedure was performed on a contact force testing platform, as shown in Figure 5(b) using the schematic shown in Figure 5(c). This platform was designed to ensure the stability and immobility of the actuator throughout the evaluation.

A bending angle test was performed to assess the actuator deformation under different air intakes. The experiment was conducted on a flat surface, as shown in Figure 5(d) using the schematic shown in Figure 5(e). The angle between the base and tip actuator was measured using a protractor, allowing analysis of the actuator's kinematic response and range of motion.

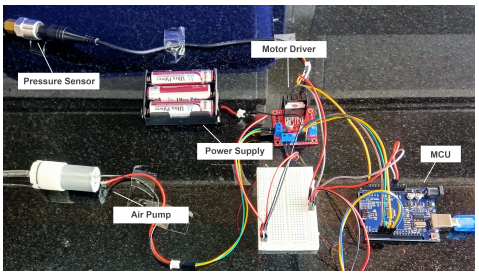

(a)

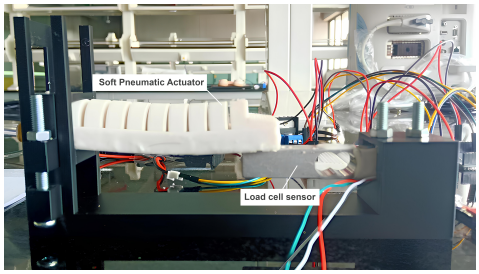

(b)

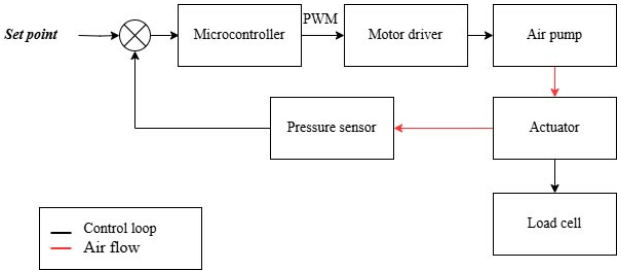

(c)

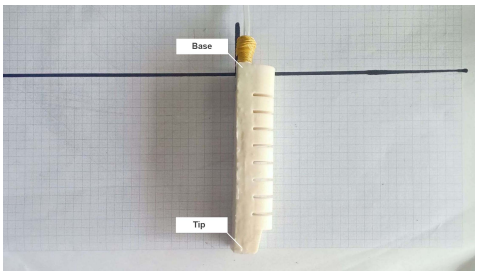

(d)

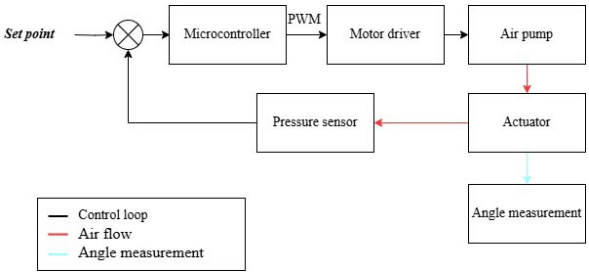

(e)

Figure 5. Experimental setup (a) data acquisition and operating system, (b) contact force platform, (c) contact force schematic, (d) bending angle platform, and (e) bending angle schematic

3. RESULTS AND DISCUSSION

3.1. Contact force measurement

Air pressure application to the Pneu-Nets actuators deforms the internal chamber by increasing its volume, resulting in a bending motion. This motion produces a tip force that directly correlates to air pressure with contact force. Figure 6(a) shows the predicted and measured tip forces up to 30 kPa, while Figure 6(b) extends the experiment to the actuator's operating limit of 52 kPa. Both curves show proportional input pressure and contact force relationships, demonstrating the consistency between simulation and experiment.

Three actuators were fabricated, and each was tested five times under identical experimental conditions (n=15). Mean, standard deviation, and 95% confidence interval (CI) were calculated for each pressure level, as summarized in Table 4. Low standard deviation ($\leq$ 0.03N) and narrow confidence intervals indicate good repeatability across trials and samples.

Within the range of 0-30 kPa, the experimental and simulated curves have an almost linear relationship. At 30 kPa, the measured contact force was 0.33 N, while the simulation predicted 0.36 N (8.3% deviation). This deviation falls within the range reported in the literature for soft pneumatic actuators. Zhong *et al.* [22] reported a deviation between simulation and experiment of 8-12%. This deviation is acceptable for soft actuator models, as it is a result of the simplification of material hyperelasticity.

Above 30 kPa, the experimental curve rises sharply, reaching 0.93 N at 52 kPa, as shown in Figure 6(b). This behavior reflects the conversion of pressure into bending and tip force after chamber ex-

pansion. By achieving almost 1 N of contact force at 52 kPa, this actuator demonstrated its ability to operate under low pressure, which is suitable for wearable rehabilitation devices.

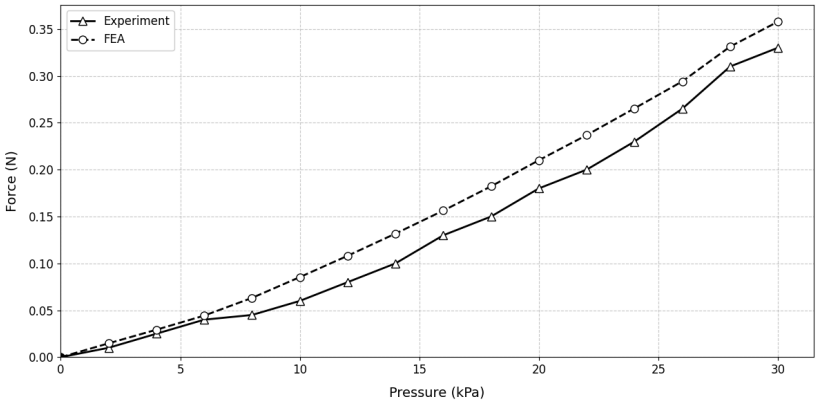

(a)

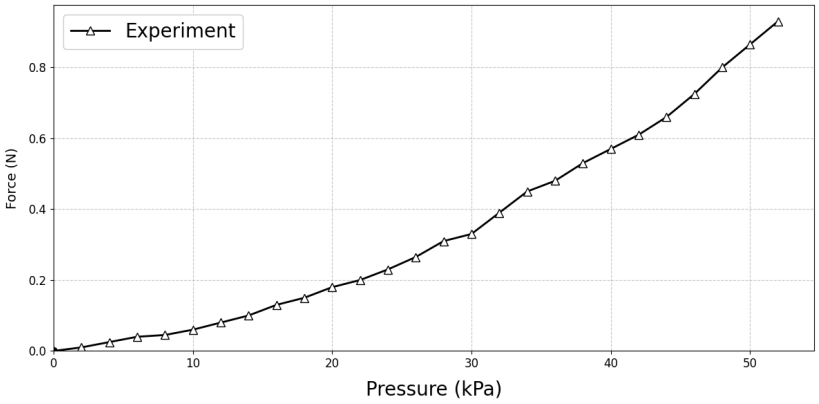

(b)

Figure 6. Contact force analysis (a) FEA and experimental result at 30 kPa and (b) experimental setup at 52 kPa

Table 4. Statistical summary of contact force measurements at 0–52 kPa (n = 15 per pressure level)

Pressure (kPa)	0	2	4	6	8	10	12	14	16	18	20	22	24	
Mean Force (N)	0	0.010	0.030	0.040	0.050	0.060	0.080	0.100	0.130	0.150	0.180	0.200	0.230	
Std. Dev (N)	0	0.001	0.002	0.002	0.003	0.003	0.004	0.004	0.004	0.005	0.005	0.006	0.006	
95% CI (±N)	0	0.001	0.001	0.001	0.002	0.002	0.002	0.002	0.002	0.002	0.002	0.003	0.003	
Pressure (kPa)	26	28	30	32	34	36	38	40	42	44	46	48	50	52
Mean Force (N)	0.270	0.310	0.330	0.390	0.450	0.480	0.530	0.570	0.610	0.660	0.725	0.800	0.865	0.930
Std. Dev (N)	0.007	0.007	0.007	0.008	0.009	0.010	0.011	0.012	0.013	0.014	0.015	0.018	0.020	0.021
95% CI (±N)	0.003	0.003	0.003	0.004	0.004	0.004	0.005	0.005	0.006	0.006	0.007	0.008	0.009	0.010

3.2. Bending angle

The bending behavior of the Pneu-Nets actuator was characterized both numerically and experimentally to determine its kinematic response. Each actuator specimen underwent five contact force measurements before three bending angle test repetitions. Because the first evaluation (contact force) employed a constrained configuration was employed that limited deformation, while the bending test allowed unrestricted movement, resulting in larger strains. As the bending angle test often damages the actuator, this test was considered a destructive experiment.

Initially, both the model and the prototype actuator remain straight, confirming that the mesh and boundary conditions do not cause excessive deformation. At 30 kPa, the actuator bends notably as the sim-

ulation predicts 202° illustrated in Figure 7(a), while the experiment records 163.3° Figure 7(b), resulting in a 19.3% error. This discrepancy is caused by the fatigue factor. Libby *et al.* [36] reported that the elastomer accuracy might drop to 80% after fatigue. Table 5 summarizes the statistical results of the bending angle. Figure 7(c) shows the pressure-angle relationship up to 30 kPa in both simulation and experiment. These curves rise as the air pressure increases and match closely up to 5 kPa. However, beyond this point, the gap between FEA and experiment results widens, indicating that the hyperelastic behavior of elastomer is not sufficiently captured in the simulation.

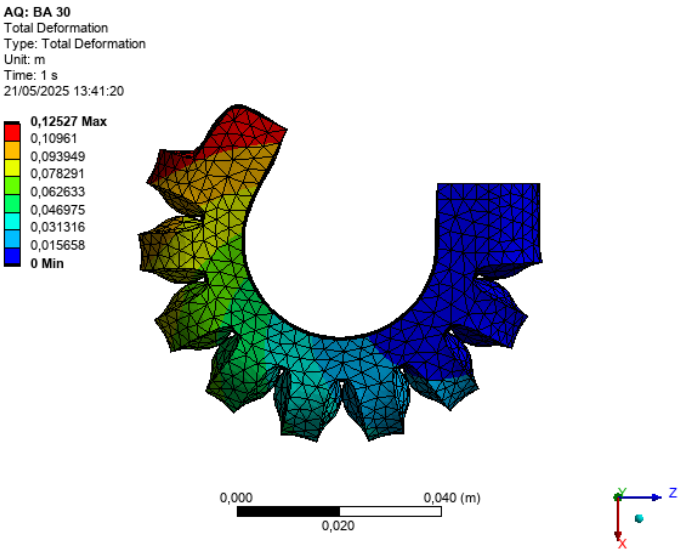

(a)

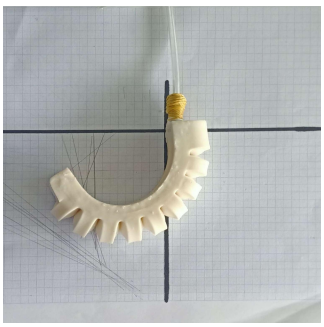

(b)

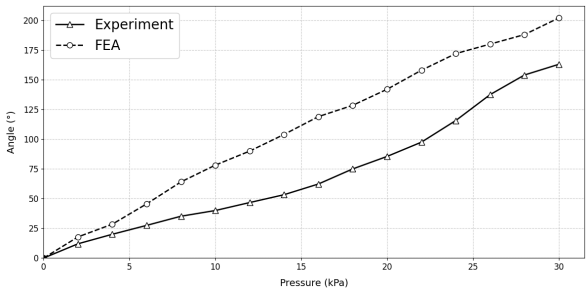

(c)

Figure 7. Bending angle analysis at 30 kPa (a) FEA simulation, (b) experimental result, and (c) comparison between FEA and experimental bending angles

Table 5. Statistical summary of bending angle measurements at 0–52 kPa (n = 9 per pressure level)

Pressure (kPa)	0	2	4	6	8	10	12	14	16	18	20	22	24	
Mean Angle (°)	0.0	12.0	20.0	27.5	35.2	40.0	46.7	53.3	62.3	75.0	85.5	97.5	115.7	
Std. Dev (°)	0.0	2.0	2.0	2.5	2.5	3.0	3.0	3.5	3.5	4.0	5.0	5.0	6.0	
95% CI (±°)	0.0	1.3	1.3	1.6	1.6	2.0	2.0	2.3	2.3	2.6	3.3	3.3	3.9	
Pressure (kPa)	26	28	30	32	34	36	38	40	42	44	46	48	50	52
Mean Angle (°)	137.5	154.0	163.0	176.0	185.0	192.0	199.5	206.4	213.0	218.3	226.0	233.0	238.7	244.5
Std. Dev (°)	7.0	7.0	8.0	7.5	7.0	6.5	6.0	5.5	5.0	4.5	4.0	3.5	3.0	2.5
95% CI (±°)	4.6	4.6	5.2	4.9	4.6	4.2	3.9	3.6	3.3	2.9	2.6	2.3	2.0	1.6

Several factors likely underlie divergence. Since the model may not have captured the highly nonlinear and multiaxial nature of the deformation during the bending at higher pressure. Although physical testing was conducted, silicone may exhibit viscoelastic softening that the purely hyperelastic model cannot reproduce. Additionally, the CAD model neglects manufacturing tolerances such as minor wall-thickness variations, air pockets, or bonding seams, stiffening the actuator and restricting its curvature. In simulation, the actuator had no supporting surface, and all contact was assumed to be frictionless. In contrast, during the experiment, a paper was used as a measurement medium, adding a friction that also contributed to bending behavior. An extended actuating pressure in the experiment is shown in Figure 8. The bending angle increases almost linearly up to 25 kPa and keeps accelerating between 25 kPa and 30 kPa. The maximum bending angle achieved is 244.5° at 52 kPa. This bending angle represents the actuator's ROM, supporting its suitability for hand finger rehabilitation. Although the simulation overestimated the angle above 10 kPa, the overall trend matches the experimental data. Future studies will be focused on the refinement of the model to reduce the discrepancies.

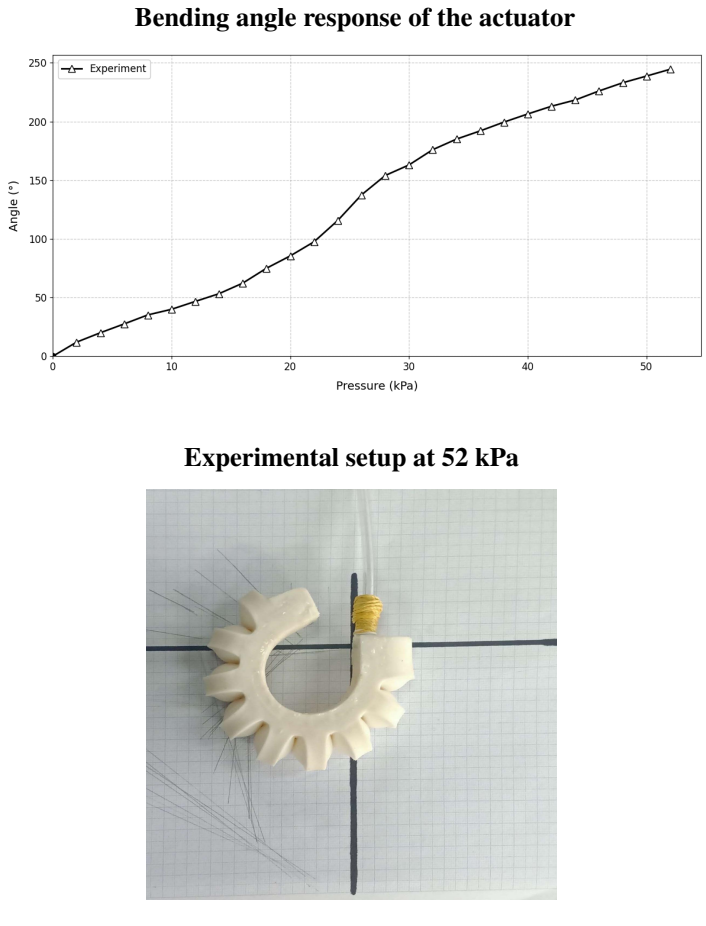

Figure 8. Bending angle response and experimental setup at 52 kPa

3.3. Preliminary design of rehabilitation gloves

A preliminary test using a master-slave control scheme confirmed the actuator's ability to support bilateral rehabilitation. The actuator was attached to the gloves at the distal (DIP), middle (MIP), and proximal interphalangeal joints (PIP). As shown in Figure 9, the actuator managed to replicate finger-bending motions, supporting its use in physical therapy and suitability for rehabilitation tasks. Since this study mainly focuses on the manufacturing and validation of the soft actuator, detailed work schemes related to mirror therapy protocols are excluded and will be discussed in future work.

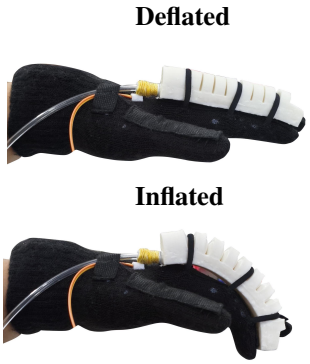

Figure 9. Preliminary study of soft rehabilitation gloves using mirror therapy

4. CONCLUSION

This study presents the design, fabrication, and characterization of a condensation-cured RTV-based Pneu-Nets actuator, which achieves large, controlled deformations at lower operating pressures than many platinum-cured actuators while maintaining structural integrity. The design consists of 10 semi-circle chambers fabricated via mold-casting. The actuator achieved a maximum bending angle of 244.5° and a tip force of 0.93 N at 52 kPa. Finite-element analysis simulations closely match the experimental results at low pressures of 5 kPa and remain within 9% and 24% error for tip force and bending angle, respectively, at 30 kPa. Confirming that the chamber design successfully distributes stress and promotes uniform wall expansion. These findings also support that condensation-cured silicone rubber is a viable, fast-curing alternative for soft-robotic actuators. Based on these findings, future development will be focused on advanced material modeling, system validation related to rehabilitation, and clinical trials on post-stroke patients.

FUNDING INFORMATION

Authors state no funding involved.

AUTHOR CONTRIBUTIONS STATEMENT

This journal uses the Contributor Roles Taxonomy (CRediT) to recognize individual author contributions, reduce authorship disputes, and facilitate collaboration.

Name of Author	C	M	So	Va	Fo	I	R	D	O	E	Vi	Su	P	Fu
Nur Rahmah Abdullah	✓	✓	✓	✓	✓	✓		✓	✓	✓	✓		✓	
Sylvi F.R. Irnadiastputri	✓	✓		✓				✓		✓		✓		
Mohammad Ikhsan	✓						✓		✓	✓		✓	✓	✓

C : **C**onceptualization
M : **M**ethodology
So : **So**ftware
Va : **Va**lidation
Fo : **Fo**rmal Analysis
I : **I**nvestigation
R : **R**esources
D : **D**ata Curation
O : Writing - **O**riginal Draft
E : Writing - Review & **E**diting
Vi : **Vi**sualization
Su : **Su**pervision
P : **P**roject Administration
Fu : **Fu**nding Acquisition

CONFLICT OF INTEREST STATEMENT

Authors state no conflict of interest.

DATA AVAILABILITY

Derived data supporting the findings of this study are available from the corresponding author MI on request.

REFERENCES

[1] D. Kuriakose and Z. Xiao, "Pathophysiology and treatment of stroke: Present status and future perspectives," *International Journal of Molecular Sciences*, vol. 21, no. 20, p. 7609, 2020, doi: 10.3390/ijms21207609.

[2] A. R. Parry-Jones *et al.*, "World Stroke Organization (WSO): Global intracerebral hemorrhage factsheet 2025," *International Journal of Stroke*, vol. 20, no. 2, pp. 145–150, Jan. 2025, doi: 10.1177/17474930241302855.

[3] J. Andersson, Å. Rejnö, S. Jakobsson, P.-O. Hansson, S. J. Nielsen, and L. Björck, "Symptoms at stroke onset as described by patients: A qualitative study," *BMC Neurology*, vol. 24, no. 1, p. 150, May 2024, doi: 10.1186/s12883-024-03652-5.

[4] D. B. Smith, S. H. Scott, J. A. Semrau, and S. P. Dukelow, "Impairments of the ipsilesional upper-extremity in the first 6-months post-stroke," *Journal of NeuroEngineering and Rehabilitation*, vol. 20, no. 1, p. 106, Aug. 2023, doi: 10.1186/s12984-023-01228-1.

[5] F. Vanoglio, L. Comini, M. Gaiani, G. P. Bonometti, A. Luisa, and P. Bernocchi, "A sensor-based upper limb treatment in hemiplegic patients: Results from a randomized pilot study," *Sensors*, vol. 24, no. 8, p. 2574, 2024, doi: 10.3390/s24082574.

[6] A. W. Dromerick *et al.*, "Critical period after stroke study (CPASS): A phase II clinical trial testing an optimal time for motor recovery after stroke in humans," *Proceedings of the National Academy of Sciences*, vol. 118, no. 39, p. e2026676118, 2021, doi: 10.1073/pnas.2026676118.

[7] S. Li, "Stroke recovery is a journey: Prediction and potentials of motor recovery after a stroke from a practical perspective," *Life*, vol. 13, no. 10, p. 2061, 2023, doi: 10.3390/life13102061.

[8] A. D. Banyai and C. Brişan, "Robotics in physical rehabilitation: Systematic review," *Healthcare*, vol. 12, no. 17, p. 1720, Aug. 2024, doi: 10.3390/healthcare12171720.

[9] D. Y.-L. Lim, H.-S. Lai, and R. C.-H. Yeow, "A bidirectional fabric-based soft robotic glove for hand function assistance in patients with chronic stroke," *Journal of NeuroEngineering and Rehabilitation*, vol. 20, no. 1, p. 120, Sep. 2023, doi: 10.1186/s12984-023-01243-2.

[10] F. Gerges, J. Desai, J. Watkins, and S. P. Burugupally, "Master-slave control for a pneumatically actuated low pressure soft robotic glove to facilitate bilateral training for stroke patients," in *Proc. 2020 23rd International Symposium on Measurement and Control in Robotics (ISMCR)*, 2020, pp. 1–6, doi: 10.1109/ISMCR51255.2020.9263764.

[11] S. Koizumi *et al.*, "Soft robotic gloves with thin McKibben muscles for hand assist and rehabilitation," in *Proc. 2020 IEEE/SICE International Symposium on System Integration (SII)*, 2020, pp. 93–98, doi: 10.1109/SII46433.2020.9025832.

[12] T. Boka, M. N. Nikkhah, and S. A. A. Moosavian, "KNTU-RoboGlove: Design of a pneumatic soft robotic glove," in *Proc. 2023 11th RSI International Conference on Robotics and Mechatronics (ICRoM)*, 2023, pp. 470–475, doi: 10.1109/ICRoM60803.2023.10412614.

[13] Y. Wang, Z. Xie, H. Huang, and X. Liang, "Pioneering healthcare with soft robotic devices: A review," *Smart Medicine*, vol. 3, no. 1, p. e20230045, 2024, doi: 10.1002/SMMD.20230045.

[14] F. Xu and H. Wang, "Soft robotics: Morphology and morphology-inspired motion strategy," *IEEE/CAA Journal of Automatica Sinica*, vol. 8, no. 9, pp. 1500–1522, 2021, doi: 10.1109/JAS.2021.1004105.

[15] Y. Wang and Q. Xu, "Design and fabrication of a soft robotic manipulator driven by fiber-reinforced actuators," in *Proc. 2018 IEEE International Conference on Mechatronics, Robotics and Automation (ICMRA)*, 2018, pp. 157–161, doi: 10.1109/ICMRA.2018.8490539.

[16] A. Pagoli, F. Chapelle, J.-A. Corrales-Ramon, Y. Mezouar, and Y. Lapusta, "Review of soft fluidic actuators: Classification and materials modeling analysis," *Smart Materials and Structures*, vol. 31, no. 1, p. 013001, Jan. 2022, doi: 10.1088/1361-665X/ac383a.

[17] N. Gariya, P. Kumar, and M. Makkar, "Experimental study of a soft pneumatic actuator for the application of robotic gripper," in *Proc. 2023 5th International Conference on Power, Control & Embedded Systems (ICPCES)*, 2023, pp. 1–4, doi: 10.1109/ICPCES57104.2023.10076021.

[18] E. Cho **et al.**, "Characterization of mechanical and dielectric properties of silicone rubber," *Polymers*, vol. 13, no. 11, p. 1831, 2021, doi: 10.3390/polym13111831.

[19] Z. Zhang, A. D. Calderon, X. Huang, G. Wu, and C. Liang, "Design and driving performance study of soft actuators

for hand rehabilitation training," *Medical Devices: Evidence and Research*, vol. 17, pp. 237–260, Jun. 2024, doi: 10.2147/MDER.S466721.
[20] W. Hu, R. Mutlu, W. Li, and G. Alici, "A structural optimisation method for a soft pneumatic actuator," *Robotics*, vol. 7, no. 2, p. 24, 2018, doi: 10.3390/robotics7020024.
[21] C. Rieger and J. Desai, "A preliminary study to design and evaluate pneumatically controlled soft robotic actuators for a repetitive hand rehabilitation task," *Biomimetics*, vol. 7, no. 4, p. 139, 2022.
[22] G. Zhong, W. Dou, X. Zhang, and H. Yi, "Bending analysis and contact force modeling of soft pneumatic actuators with pleated structures," *International Journal of Mechanical Sciences*, vol. 193, p. 106150, 2021, doi: 10.1016/j.ijmecsci.2020.106150.
[23] P. T. Do, D. T. Vo, and H. P. Le, "A soft pneumatic robotic glove for hand rehabilitation after stroke," in *Proc. 2021 20th International Conference on Advanced Robotics (ICAR)*, 2021, pp. 7–12, doi: 10.1109/ICAR53236.2021.9659404.
[24] A. Mészáros and J. Sárosi, "Increasing the force exertion of a soft actuator using externally attachable inter-chamber plates," *Actuators*, vol. 12, no. 6, p. 222, 2023, doi: 10.3390/act12060222.
[25] J. R. Barrientos, H. W. Fabian, V. E. Abarca, and D. A. Elías, "An electro-pneumatic glove using a soft actuator for flat pinch movement in pediatric finger rehabilitation," in *Proc. 2024 IEEE 15th Latin America Symposium on Circuits and Systems (LASCAS)*, 2024, pp. 1–5, doi: 10.1109/LASCAS60203.2024.10506183.
[26] N. Gariya, P. Kumar, B. Prasad, and T. Singh, "Soft pneumatic actuator with an embedded flexible polymeric piezoelectric membrane for sensing bending deformation," *Materials Today Communications*, vol. 35, p. 105910, 2023, doi: 10.1016/j.mtcomm.2023.105910.
[27] I. Rhiu and W. Kim, "Estimation of stature from finger and phalange lengths in a Korean adolescent," *Journal of Physiological Anthropology*, vol. 38, no. 1, p. 13, Oct. 2019, doi: 10.1186/s40101-019-0203-4.
[28] W. Kim, B. Seo, S. Y. Yu, and K.-J. Cho, "Deployable soft pneumatic networks (D-PneuNets) actuator with dual-morphing origami chambers for high-compactness," *IEEE Robotics and Automation Letters*, vol. 7, no. 2, pp. 1262–1269, 2022, doi: 10.1109/LRA.2021.3137504.
[29] P. T. Do, D. T. Vo, and H. P. Le, "A soft pneumatic robotic glove for hand rehabilitation after stroke," in *Proc. 2021 20th International Conference on Advanced Robotics (ICAR)*, 2021, pp. 7–12, doi: 10.1109/ICAR53236.2021.9659404.
[30] M. Tiboni and D. Loda, "Monolithic PneuNets soft actuators for robotic rehabilitation: Methodologies for design, production and characterization," *Actuators*, vol. 12, no. 7, p. 299, 2023, doi: 10.3390/act12070299.
[31] A. Jurásková, S. M. Olsen, and A. L. Skov, "Reversible dynamic behavior of condensation-cured silicone elastomers caused by a catalyst," *Macromolecular Materials and Engineering*, vol. 308, no. 6, p. 2200615, 2023, doi: 10.1002/mame.202200615.
[32] A. Jurásková, S. M. Olsen, K. Dam-Johansen, M. A. Brook, and A. L. Skov, "Reliable condensation curing silicone elastomers with tailorable properties," *Molecules*, vol. 26, no. 1, p. 82, 2021, doi: 10.3390/molecules26010082.
[33] Z. Li, Z. Zhou, Y. Li, and S. Tang, "Effect of cyclic loading on surface instability of silicone rubber under compression," *Polymers*, vol. 9, no. 4, p. 148, 2017, doi: 10.3390/polym9040148.
[34] J. Ilg, S. J. Rupitsch, A. Sutor, and R. Lerch, "Determination of dynamic material properties of silicone rubber using one-point measurements and finite element simulations," *IEEE Transactions on Instrumentation and Measurement*, vol. 61, no. 11, pp. 3031–3038, 2012, doi: 10.1109/TIM.2012.2203449.
[35] X. Li, Y. Hao, J. Zhang, C. Wang, D. Li, and J. Zhang, "Design, modeling and experiments of a variable stiffness soft robotic glove for stroke patients with clenched fist deformity," *IEEE Robotics and Automation Letters*, vol. 8, no. 7, pp. 4044–4051, 2023, doi: 10.1109/LRA.2023.3279613.
[36] J. Libby *et al.* "What happens when pneu-net soft robotic actuators get fatigued?" in *2023 International Symposium on Medical Robotics (ISMR)*, 2023, pp. 1–6, doi: 10.1109/ISMR57123.2023.10130227.

BIOGRAPHIES OF AUTHORS

Nur Rahmah Abdullah obtained her bachelor's degree in biomedical engineering from Universitas Airlangga, Indonesia. She is currently pursuing a master's degree in biomedical engineering at Universitas Indonesia. Her research interests lie in computational modelling, finite element analysis, and rehabilitation engineering. She can be contacted at email: nur.rahmah33@ui.ac.id.

Sylvi Febriana Rachmawati Irnadiastputri received her bachelor's and master's degrees in biomedical engineering from National University of Singapore. She is currently a lecturer in Biomedical Engineering Program, Universitas Indonesia. Her research interests include tissue biomechanics, computational biology, and finite element analysis. She has experience in modelling the eye and the spine. She can be contacted at email: sylvi.febriana@office.ui.ac.id.

Mohammad Ikhsan received his bachelor's and master's degrees in electrical engineering from Bandung Institute of Technology (ITB), Indonesia. He then received his Ph.D. degree in electrical and computer engineering from the National University of Singapore (NUS), Singapore. He is currently an assistant professor with the Department of Electrical Engineering, Universitas Indonesia. His research interests include computer vision, robotics, artificial intelligence, and embedded systems. He can be contacted at email: mohammad.ikhsan04@ui.ac.id.